

ON THE DYNAMIC BUCKLING OF A SIMPLE ELASTIC-PLASTIC MODEL

NORMAN JONES† and H. L. M. DOS REIS‡

Department of Ocean Engineering, Massachusetts Institute of Technology, Cambridge, MA 02139, U.S.A.

(Received 27 September 1979; in revised form 17 March 1980)

Abstract—In order to provide some insight into the phenomenon of dynamic plastic buckling, the response of an imperfection-sensitive idealised model with elastic-plastic springs to simulate material plasticity was examined using theoretical and numerical methods.

The theoretical method predicts that dynamic plastic-elastic buckling governs the response for small imperfections, while dynamic instability occurs elastically for large imperfections. Furthermore, the dynamic buckling load of a model with small imperfections is larger than the corresponding static buckling load because of the different elastic-plastic deformation histories in the springs during the static and dynamic responses.

The numerical study reveals two distinct forms of dynamic response known as "direct" and "indirect" dynamic buckling which occur within specific ranges of the parameters.

The various results presented herein indicate that dynamic plastic buckling is imperfection-sensitive particularly for "direct" dynamic buckling.

NOTATION

a	$L_2\beta/2Kr^2$
m_0, m_1	masses defined in Fig. 1
r	L_1/L_2
t	time
u	displacement defined in Fig. 1(b)
u_1, u_2	displacements of springs 1 and 2 in Fig. 1
y_0	vertical displacement in Fig. 1(b)
y	y_0/L_2
z, \bar{z}	$\xi/L_2, \bar{\xi}/L_2$
z_y	defined by eqn (26)
z^*	maximum value of z
F_1, F_2	forces in springs 1 and 2, respectively
K, K_t	spring coefficients defined in Fig. 2
L_1, L_2	length of members shown in Fig. 1(a)
P	total vertical load as shown in Fig. 1(b)
P_c	Euler buckling load (eqn 5)
P_D	dynamic buckling load
P_m	reduced modulus load (eqn 7)
P_t	tangent modulus load (eqn 6)
P^*	maximum load
Q_1, Q_2, Q	defined by eqns 4(j-1), respectively
β	characteristic for softening non-linear spring at A in Fig. 1(b)
ϵ	ω_1^2/ω_0^2
λ	K_t/K
ξ	horizontal displacement of A in Fig. 1(b)
ξ	initial imperfection indicated in Fig. 1(a)
τ	$\omega_1 t$
ω_0^2	$2K/m_0$
ω_1^2	$2Kr^2/m_1$
Δ_y	displacement at yield in springs 1 and 2
$\Delta\tau$	non-dimensional time step in numerical analysis
Ω	$\lambda/(1+\lambda)$
(γ)	$\partial(\)/\partial\tau$

†Present address: Department of Mechanical Engineering, University of Liverpool, P.O. Box 147, Brownlow Hill, Liverpool L69 3BX, England.

‡Present address: Department of General Engineering, University of Illinois, Transportation Building, Urbana, IL 61801, U.S.A.

1. INTRODUCTION

The phenomenon of dynamic plastic buckling, which is characterised by wrinkling as in static buckling, may occur when structures are subjected to large external dynamic loads. It usually develops during motor vehicle, train, aircraft and ship collisions and is of some interest in aerospace, nuclear and petroleum engineering.

Perturbation methods of analysis have been used to explore successfully the unstable dynamic plastic response of rods impacted axially[1], rectangular plates subjected to in-plane loads[2, 3], cylindrical shells and rings acted on by various dynamic loads[4-6, etc.] and spherical shells loaded impulsively[7, 8]. This theoretical procedure is predicated on the assumption that the characteristic wrinkling of structures associated with dynamic buckling develops from initial imperfections in the geometry or impulsive velocity fields. Reference[6] contains some comparisons between the theoretical predictions of perturbation analyses and experimental results for cylindrical shells and rings loaded impulsively. Generally speaking, these comparisons and those for several other structures show that the perturbation method may provide reasonable estimates of the corresponding experimental values which are adequate for design purposes. However, there are many dynamic plastic buckling problems for which the perturbation method of analysis is unsuitable. These problems could be examined using numerical schemes [9-11]. Unfortunately, it is an expensive and time-consuming exercise to seek dynamic buckling loads with wholly numerical methods[12] so that valuable insight into the general problem of dynamic plastic buckling is often lacking. Furthermore, Hartzman[9] found that the dynamic buckling pressure of a particular elastic-plastic perfect spherical dome was larger than the corresponding static collapse pressure in contradistinction to the observations of other authors for elastic caps subjected to step pressures of unlimited duration[13].

Shanley[14] examined the behavior of a simple idealised model and obtained valuable insight into the static inelastic buckling of a column. Sewell[15] discussed this topic further, while Hutchinson[16] has explored the potential importance of initial geometric imperfections on the static plastic buckling of a simple model. The influence of initial geometric imperfections on the dynamic buckling of a simple elastic models has been investigated by Budiansky and Hutchinson [17-19] and Danielson[20]. Huang and Tsai[21] used a phase-plane procedure to investigate the dynamic snap-through behavior of a simple shallow elastic perfectly plastic truss without bending and axial inertia effects.

In an attempt to gain some insight into the simultaneous influence of material plasticity and initial geometric imperfections on dynamic buckling, a theoretical study is presented for the idealised elastic linear work hardening imperfection-sensitive model shown in Fig. 1. This

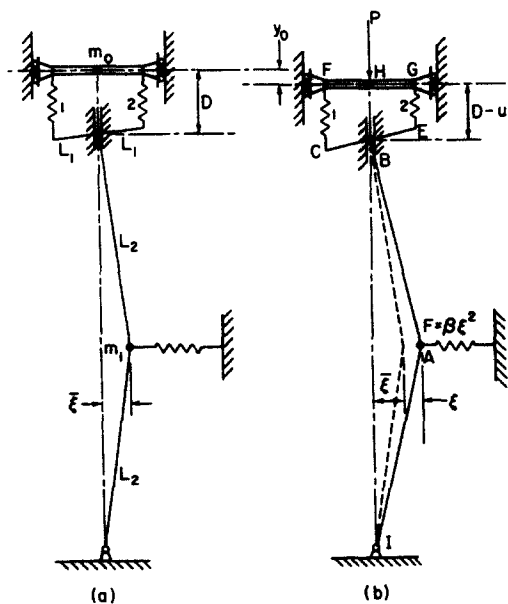


Fig. 1. Simple model. (a) Initial position; (b) Deformed position.

idealised model is similar to that employed by Danielson[20], except that it is modified to include the influence of material plasticity in a manner similar to Hutchinson[16] for static loads.

2. BASIC EQUATIONS

The simple model shown in Fig. 1(a) was constructed by combining the essential features of the models used in Refs. [16, 20]. Danielson used the imperfection-sensitive model illustrated in Fig. 1 of Ref.[20] to study the characteristics of dynamic elastic buckling, while the imperfection-sensitive model in Fig. 1 of Ref.[16] allowed Hutchinson to explore the static postbuckling behaviour in the plastic range.

The various members in Fig. 1(a) are rigid and weightless and the only masses, m_0 and m_1 , are concentrated at H and A , respectively. The unloaded model has a stress-free initial imperfection $\bar{\xi}$, while the member FHG is constrained to remain horizontal. Member FHG and pin B are constrained to move vertically in frictionless guides. Frictionless pins are located at A , B and I and the behavior of the softening non-linear spring at A is governed by the relation $F = \beta\xi^2$, where $\xi + \bar{\xi}$ is the total horizontal displacement of A as indicated in Fig. 1(b). The material behavior is simulated by springs 1 and 2 with the load-displacement characteristics shown in Fig. 2 and, for convenience, it is assumed that the springs have identical characteristics.

Now, it is straightforward to show that the deformations of springs 1 and 2 are

$$u_1 = u - r\xi \quad \text{and} \quad u_2 = u + r\xi, \quad \text{respectively,} \tag{1a, b}$$

where

$$u = y_0 - \xi(\xi + 2\bar{\xi})/L_2 \tag{2}$$

provided $(\xi + \bar{\xi})/L_2 \ll 1$. The equations of motion may be written in the dimensionless form

$$\epsilon y'' + r^2(Q_1 + Q_2)/2 = r^2 Q/2 \tag{3a}$$

and

$$z'' - (z + \bar{z})(Q_1 + Q_2) - r(Q_1 - Q_2)/2 - az^2 = 0, \tag{3b}$$

when neglecting the vertical acceleration of m_1 , and where

$$\begin{aligned} y &= y_0/L_2, \quad z = \xi/L_2, \quad \bar{z} = \bar{\xi}/L_2, \quad r = L_1/L_2, \quad \omega_0^2 = 2K/m_0, \\ \omega_1^2 &= 2Kr^2/m_1, \quad \epsilon = \omega_1^2/\omega_0^2, \quad a = L_2\beta/2Kr^2, \quad P_c = KrL_1, \\ Q_1 &= F_1/P_c, \quad Q_2 = F_2/P_c, \quad Q = P/P_c, \quad \tau = \omega_1 t, \quad \text{and} \\ ()' &= \partial()/\partial\tau. \end{aligned} \tag{4a-m}$$

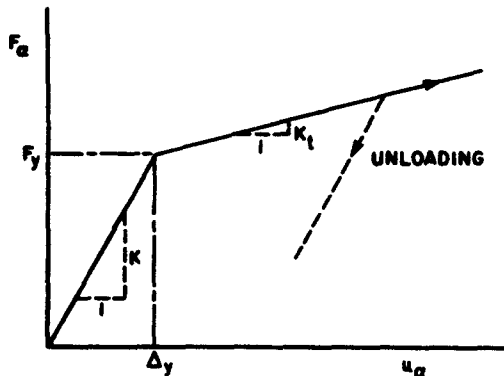


Fig. 2. Elastic-plastic characteristics of springs 1 and 2.

F_1 and F_2 are the forces in springs 1 and 2, respectively, while P is the external load applied at H .

3. STATIC BEHAVIOR

The equations in the foregoing section predict that the static elastic Euler buckling load for a perfect model (i.e. $\bar{\xi} = 0$) is

$$P_c = KrL_1, \tag{5}$$

while the tangent modulus buckling load is

$$P_t = K_t r L_1. \tag{6}$$

The reduced modulus load is

$$P_m = 2KK_t r L_1 / (K + K_t) \tag{7}$$

and occurs when bifurcation takes place with no change of the external load.

It is found for the imperfect case (i.e. $\bar{\xi} \neq 0$) that

$$P/P_c = z(1 - az)/(z + \bar{z}) \tag{8}$$

when springs 1 and 2 remain elastic. Thus,

$$(1 - P^*/P_c)^2 = (4a\bar{z})(P^*/P_c), \tag{9}$$

where P^* is the maximum load (buckling load) which occurs at the associated displacement

$$z^* = -\bar{z} + (\bar{z}^2 + \bar{z}/a)^{1/2}. \tag{10}$$

If \bar{z} is sufficiently small, then eqns (9) and (10) predict

$$P^*/P_c \approx 1 - (4a\bar{z})^{1/2}, \quad \bar{z} \geq 0. \tag{11}$$

The elastic characteristics of the simple model in Fig. 1(a) according to the above equations are illustrated in Fig. 3.

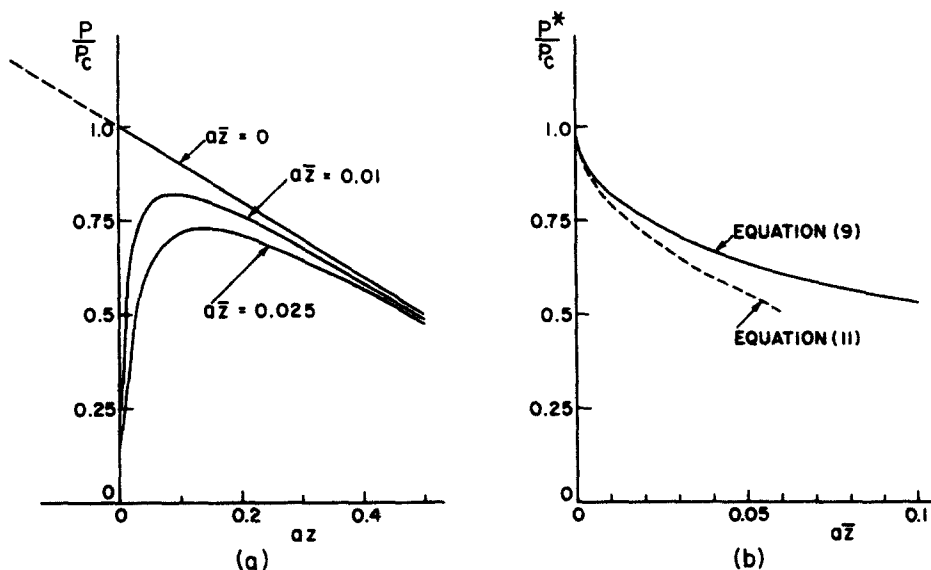


Fig. 3. Static elastic characteristics of simple model, (a) eqn (8), (b) eqns (9) and (11).

Spring number 2 first commences to respond plastically when $u_2 = \Delta_p$, where Δ_p is defined in Fig. 2. If the initial imperfection amplitude ($\bar{\xi}$) is sufficiently small, then loading continues with spring number 2 deforming plastically and spring number 1 remaining elastic until eventually spring number 1 becomes plastic when $u_1 = \Delta_p$. Further loading continues with both springs responding plastically until spring number 1 commences to unload elastically. Finally, spring number 2 continues to load plastically and spring number 1 unloads elastically from its earlier plastic state.

The maximum load P^* may be expressed in the form

$$P^* = P_0^* - \beta L_2^2 \{ \hat{z} + [(1 + 4K_1 L_1 / \beta L_2^2)^{1/2} - 1](\hat{z} + \bar{z}) \}, \tag{12}$$

where

$$\hat{z} = -\bar{z} + \{ \bar{z}^2 + \bar{z}(r - 2\bar{z})(1 + \beta L_2^2 / 4K_1 L_1)^{-1/2} \}^{1/2} \tag{13}$$

is the value of z when spring number 1 commences to unload elastically and P_0^* is the maximum load that the simple perfect ($\bar{\xi} = 0$) model can support. If bifurcation occurs at the tangent modulus load given by eqn (6), then

$$P_0^* = P_i [1 + \lambda(1 - \lambda) / \{ ar(1 + \lambda) \} + \dots] \tag{14}$$

and

$$P^* / P_0^* \approx 1 - (4a\bar{z} / \lambda)^{1/2} \tag{15}$$

for sufficiently small values of \bar{z} , where

$$\lambda = K_1 / K. \tag{16}$$

The analysis of this sequence of loading which leads to eqns (12)–(15) is quite straightforward but the details are not presented here because Sewell[15] and Hutchinson[16] have discussed the static plastic behavior of simple models without and with initial imperfections, respectively. In fact, eqns (12)–(15) are respectively similar to eqns (11), (10), (9)† and (12) in Ref.[16]. The general features of the response sketched in Fig. 4 for this simple model confirm the characteristics observed by Hutchinson for the model shown in Fig. 1 of Ref.[16]. However, of particular interest is the observation that eqns (11) and (15) demonstrate that the

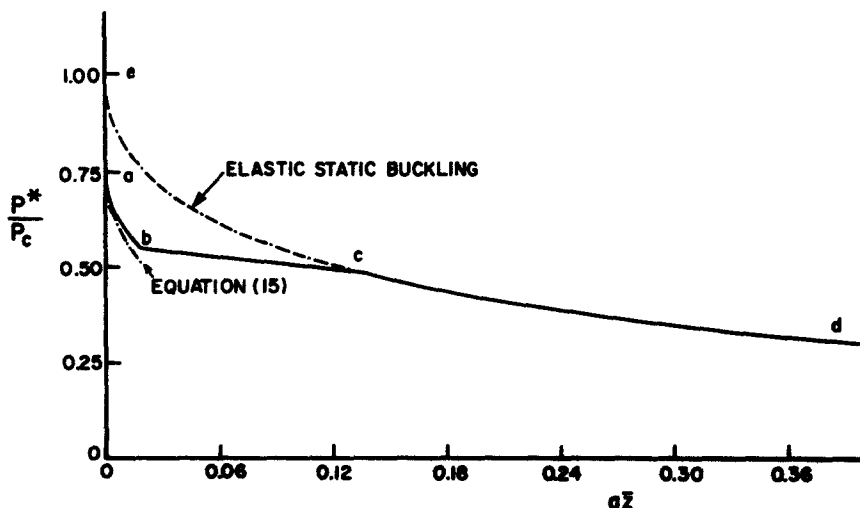


Fig. 4. Static buckling loads of idealized model according to eqn (9) (acd, elastic), eqns (12) and (13) (ab), and curve bc is obtained with spring number 1 elastic and spring number 2 plastic. $a = 10$, $r = 1$, $\lambda = 0.75$ and $\Delta_p L_2 / L_1^2 = 0.266$.

†The analogy between the variables here and in Ref.[16] shows that the equation following Hutchinson's eqn (9) has $2ar$ instead of ar as in eqn (14) here.

simple model is more imperfection sensitive in the plastic range than in the elastic range because an imperfection amplitude ΔF gives rise to the same relative reduction of the buckling load as does \bar{z} in the elastic case. It is also evident from Fig. 4, for example, that an imperfection may cause the simple model to buckle in a wholly elastic manner even though the perfect model would buckle plastically. An interested reader is referred to Ref. [16] for further discussion.

4. DYNAMIC BEHAVIOUR WITH $m_0 = 0$

The dynamic behaviour of the simple model in Fig. 1 with $m_0 = 0$ when subjected to a step loading of constant magnitude and infinite duration is explored in this section using a theoretical analysis.

Equation (3a) with $\epsilon = 0$ (i.e. $m_0 = 0$) predicts

$$Q_1 + Q_2 = Q \tag{17a}$$

so that eqn (3b) becomes

$$z'' - Q(z + \bar{z}) - r(Q_1 - Q_2)/2 - az^2 = 0 \tag{17b}$$

with the associated initial conditions

$$z(0) = z'(0) = 0. \tag{17c, d}$$

The characteristics of springs 1 and 2 are identical and are illustrated in Fig. 2.

4.1 Wholly elastic response

If it is assumed that the model remains elastic throughout the response then the forces in springs 1 and 2 are respectively

$$F_1 = K(u - rL_2z) \quad \text{and} \quad F_2 = K(u + rL_2z) \tag{18a, b}$$

according to eqns (1). Thus,

$$u = P/2K \tag{19a}$$

when using eqn (17a) and

$$F_1 - F_2 = -2KL_2rz, \tag{19b}$$

so that eqn (17b) becomes

$$z'' + (1 - P/P_c)z - az^2 = \bar{z}P/P_c \tag{20}$$

which gives

$$z'^2 + (1 - P/P_c)z^2 - 2az^3/3 = 2\bar{z}zP/P_c \tag{21}$$

when satisfying eqns (17c, d).

Equation (20) is an autonomous equation so that it is suitable for a phase plane analysis using the variables z' and z [22]. It is straightforward to show that there are two singular points on the z axis ($z' = 0$) one of which is a center or vortex point and the other a saddle point according to the stability theorem [23]. The maximum value of $z = z^*$ occurs when $z' = 0$ in eqn (21) and is given by

$$z^* = 3[(1 - P/P_c) \pm \{(1 - P/P_c)^2 - 16a\bar{z}P/3P_c\}^{1/2}]/4a. \tag{22}$$

The largest possible value of P/P_c occurs when the radical in eqn (22) is zero, or

$$(1 - P_D/P_c)^2 = 16a\bar{z}P_D/3P_c, \tag{23}$$

where P_D is the dynamic buckling load. Equation (23) is also found from eqn (21) with $z' = 0$ when differentiating with respect to z , then substituting $z = z^*$ and $dP/dz^* = 0$. Moreover, the value of z^* according to eqn (22) with P_D given by eqn (23) coincides with the saddle point on the z axis in the $z' - z$ phase plane.

Now, in order for the foregoing analysis to remain valid it is necessary that springs 1 and 2 behave elastically throughout the entire response. This is assured if the force in spring number 2 remains less than the yield force ($F_2 = K\Delta_y$), or

$$P_D/P_c \leq (4a\Delta_y/3L_1 - 1)(2ar/3 - 1)^{-1} \tag{24}$$

according to eqns (18b), (19a), (22) and (23).

Budiansky and Hutchinson examined the dynamic elastic buckling of the idealised column shown in Fig. 3 of Ref. [17] and uncovered a buckling criterion identical to eqn (23). Incidentally, if \bar{z} in eqn (23) is eliminated using eqn (9), then

$$P_D/P^* = 0.75\{(1 - P_D/P_c)/(1 - P^*/P_c)\}^2 \tag{25}$$

which as remarked in Ref. [17] gives $0.75 \leq P_D/P^* \leq 1$, the lower values of P_D being associated with the more imperfect model.

4.2 Elastic-plastic response

It is evident for sufficiently large loads that plastic flow first occurs in spring number 2 just as motion ceases according to equality (24). Thus, dynamic loads which violate inequality (24) cause plastic flow in spring number 2 at some intermediate time during the response. This suggests that the elastic analysis in Section 4.1 remains valid during a first phase of motion up to some time when $u_2 = \Delta_y$, or

$$z_y = \Delta_y/L_1 - rP/2P_c. \tag{26}$$

The subsequent response is controlled by plastic behaviour in spring number 2, while spring number 1 remains elastic.

The spring forces are therefore

$$F_1 = \bar{F}_1 + K(u_1 - \bar{u}_1), \quad \text{and} \quad F_2 = \bar{F}_2 + K_1(u_2 - \bar{u}_2) \tag{27a, b}$$

during the second stage of motion, where all the barred quantities are evaluated at the end of the first stage of motion. It is straightforward to show that

$$F_1 - F_2 = (K - K_1)u - rL_2(K + K_1)z - (K - K_1)\Delta_y, \tag{28a}$$

where

$$u = rL_2z(K - K_1)/(K + K_1) + P/(K + K_1) - \Delta_y(K - K_1)/(K + K_1). \tag{28b}$$

Thus, eqns (17b), (26) and (28a) give

$$z'' + Az - az^2 = B/4a, \quad z \geq z_y, \tag{29}$$

where

$$A = 2\Omega - P/P_c, \quad \Omega = \lambda/(1 + \lambda), \quad \text{and} \\ B = 4a\{zP/P_c - (1 - \lambda)z_y/(1 + \lambda)\}. \tag{30a-c}$$

The phase plane method can be used to study eqn (29) and show that two singular points occur on the z axis at

$$z_{1,2} = (A \pm \sqrt{(A^2 - B)})/2a, \quad (31a, b)$$

where z_1 is a saddle point and z_2 is a center or vortex point.

The first integral of eqn (29) is

$$z'^2 + Az^2 - 2az^3/3 = Bz/2a + (1 - \lambda)z^2/(1 + \lambda), \quad (32)$$

where the constant of integration was found by matching z' at the start of the second phase of motion with eqn (21) at z_y . The greatest value of z (say z^*) on a closed trajectory in the phase plane occurs when $z' = 0$, or

$$Az^{*2} - 2az^{*3}/3 = Bz^*/2a + (1 - \lambda)z^{*2}/(1 + \lambda). \quad (33)$$

If the location of the saddle point z_1 given by eqn (31a) is identified with z^* , then eqn (33) gives

$$2\{A^3 + (A^2 - B)^{3/2}\}/3 - AB - (2az_y)^2(1 - \lambda)/(1 + \lambda) = 0, \quad (34)$$

where P in eqns (30a) and (30c) for A and B is identified with the dynamic buckling load (P_D). It should be noted that $z'' = 0$ according to eqn (29) with $z = z_{1,2}$ given by eqns (31).

Now, the foregoing theoretical analysis is valid provided $z_y \geq 0$, or $u \leq \Delta_y \dagger$, which leads to

$$P_D/P_c \leq 2\Delta_y/rL_1, \quad (35)$$

according to eqn (26). Moreover, P_D/P_c must be larger than the r.h.s. of inequality (24) so that this analysis remains valid when

$$(4a\Delta_y/3L_1 - 1)(2ar/3 - 1)^{-1} \leq P_D/P_c \leq 2\Delta_y/rL_1. \quad (36)$$

4.3 Plastic-elastic response

The equality (35) is associated with $u = \Delta_y \dagger$ which implies that springs 1 and 2 reach the yield force ($K\Delta_y$) when $\xi = 0$. Thus, dynamic loads which violate inequality (35) would give rise to plastic behavior in both springs prior to the motion of mass m_1 . The force in each spring is equal when $\xi = 0$ so that both must be either elastic as in Sections 4.1 and 4.2 or plastic as in the present case. However, once m_1 commences motion (i.e. $\xi > 0$) it is evident from eqns (1) that spring 1 must unload elastically, while spring 2 continues to load plastically. In this circumstance it may be shown that

$$F_1 - F_2 = -4rKK_tL_2z/(K + K_t) \quad (37a)$$

and

$$\dot{u} = P/2K_t + (1 - K/K_t)\Delta_y \quad (37b)$$

is the compression of the springs immediately prior to the onset of motion of mass m_1 .

Equations (17b) and (37a) give

$$z'' + (2\Omega - P/P_c)z - az^2 = \bar{z}P/P_c \quad (38)$$

the solution of which must satisfy the initial conditions (17c, d). If eqn (38) is solved in a manner similar to the elastic case outlined in Section 4.1 here then

$$z'^2 + (2\Omega - P/P_c)z^2 - 2az^3/3 = 2z\bar{z}P/P_c \quad (39a)$$

$\dagger u$ refers to the first phase of motion and is given by eqn (19a).

and the dynamic buckling load is given by the expression

$$(2\Omega - P_D/P_c)^2 = 16a^2P_D/3P_c \tag{39b}$$

which reduces to eqn (23) when $\lambda = 1$.

The foregoing analysis remains valid provided $P_D/P_c \geq 2\Delta_j/rL_1$ according to inequality (36). Furthermore, we note eqn (39b) requires $P_D/P_c \leq 2\Omega$ so that

$$2\Delta_j/rL_1 \leq P_D/P_c \leq 2\Omega \tag{40}$$

in order for this analysis to be appropriate.

If the dimensionless initial imperfection (\bar{z}) is eliminated from eqn (39b) using the approximate expression for the maximum static load (P^*) of the imperfect model (eqn 15), then for sufficiently small values of \bar{z}

$$P_D/P_c \approx 0.75(2\Omega - P_D/P_c)^2 / \{\lambda(1 - P^*/P_c^*)^2\}, \tag{41}$$

where P_c^* is the maximum static load of the perfect model which is given by eqn (14). Equation (41) with $\lambda = 1$ reduces to the corresponding equation for the dynamic elastic case which is obtained from eqns (11) and (23) when \bar{z} is small.

A comparison of eqns (23) and (39b) reveals that the load associated with dynamic buckling of the model in the plastic range is smaller than that required when both springs remain elastic.

5. UNLOADING WITH $m_0 = 0$

The theoretical analysis in Section 4.1 for the wholly elastic response of the idealised model in Fig. 1 remains valid for any reversed loading in springs 1 and 2 (i.e. $z' < 0$) so that a complete phase plane portrait may be constructed as shown in Fig. 5 for a particular case. However, the analyses for dynamic elastic-plastic and plastic-elastic behavior in Sections 4.2 and 4.3, respectively, only remain valid provided $z' \geq 0$. The deformations of springs 1 and 2 can reverse and unload elastically when $z' \leq 0$ leaving the springs stretched permanently as indicated in Fig. 2. The theoretical study in this section investigates the influence of elastic unloading in the dynamic elastic-plastic and plastic-elastic cases to allow for completion of the phase-plane portraits.

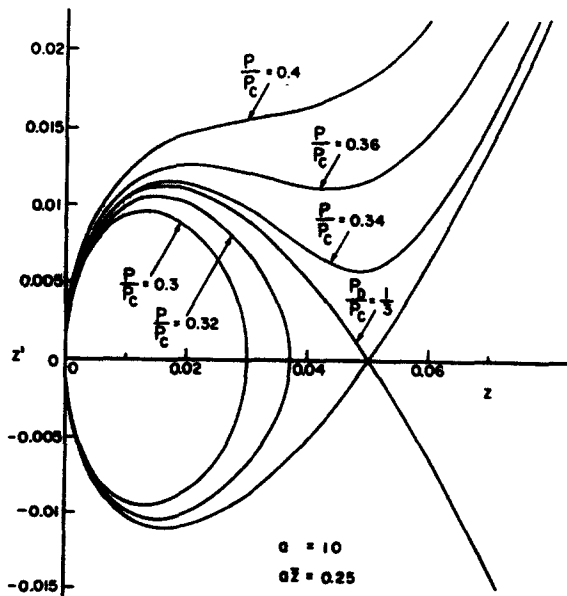


Fig. 5. Phase plane trajectories for the dynamic elastic case with $m_0 = 0$. Equations (21) and (23) with $a = 10$, and $aZ = 0.25$.

5.1 *Elastic-plastic case*

It is evident from the theoretical study in Section 4.2 that spring number 1 in Fig. 1(a) remains elastic throughout motion, while spring 2 is elastic initially during the first phase of motion but behaves plastically when $z \geq z_y$ and $z' \geq 0$ during a second phase of motion, where z_y is given by eqn (26). The forces (F_1^* , F_2^*) in springs 1 and 2 at the end of the second phase of motion are given by eqns (27) with $z' = 0$. If it is assumed that the subsequent behaviour of both springs is elastic during a third phase of motion, then

$$F_1 = K(u^* - rL_2z), \quad \text{and} \quad F_2 = F_2^* - K(u_2^* - u_2), \tag{42a, b}$$

where all variables with $z' = 0$ at the end of the second phase of motion are indicated with an asterisk (*).

It may be shown that eqns (1), (4), (5), (16), (27), (28b), and (42) give

$$Q_1 - Q_2 = 2(1 - \lambda)z^*/r(1 + \lambda) + (1 - \lambda)Q/(1 + \lambda) - 2z/r - 2(1 - \lambda)\Delta_y\{rL_1(1 + \lambda)\}, \tag{43}$$

which allows eqn (17b) to be written

$$z'' + (1 - Q)z - az^2 = (1 - \lambda)(z^* + rQ/2 - \Delta_y/L_1)/(1 + \lambda) + \bar{z}Q. \tag{44}$$

The solution of eqn (44) which satisfies the conditions $z = z^*$ and $z' = 0$ at the start of the third phase of motion is

$$z'^2 + (1 - Q)z^2 - 2az^3/3 = Cz + D, \tag{45}$$

where

$$C = 2\bar{z}Q + 2(1 - \lambda)(z^* - z_y)/(1 + \lambda) \tag{46a}$$

and

$$D = (1 - \lambda)(z_y^2 - z^{*2})/(1 + \lambda) \tag{46b}$$

when using eqn (32) to give z^* .

Springs 1 and 2 remain elastic throughout the third stage of motion provided $(u^* - \Delta_y) \leq rL_2z \leq rL_2z^*$, or

$$(1 - \lambda)z^*/(1 + \lambda) - 2z_y/(1 + \lambda) \leq z \leq z^*. \tag{47}$$

5.2 *Plastic-elastic case*

It is evident from Section 4.3 that both springs 1 and 2 immediately respond plastically due to a sufficiently large step loading P , but spring 1 then unloads elastically when motion commences, while spring 2 continues to behave plastically. Thus, the response examined in Section 4.3 consists of a single phase of motion which terminates when $z = z^*$, where z^* is given by eqn (39a) with $z' = 0$.

If it is assumed that the subsequent response of the idealised model in Fig. 1 is governed by elastic behavior in springs 1 and 2, then

$$F_1 = P/2 + KrL_2(K - K_t)z^*/(K + K_t) - KrL_2z \tag{48a}$$

and

$$F_2 = P/2 - KrL_2(K - K_t)z^*/(K + K_t) + KrL_2z, \tag{48b}$$

where all variables with an asterisk (*) are evaluated when $z' = 0$ and $z = z^*$. Thus, substituting eqns (4), (5), (16) and (48) into eqn (17b) gives

$$z'' + (1 - Q)z - az^2 = Q\bar{z} + (1 - \lambda)z^*/(1 + \lambda) \tag{49}$$

which has the solution

$$z^2 + (1 - Q)z^2 - 2az^3/3 = Ez + F \quad (50)$$

when satisfying $z' = 0$ at $z = z^*$ and where

$$E = 2Q\bar{z} + 2(1 - \lambda)z^*/(1 + \lambda) \quad (51a)$$

$$F = -(1 - \lambda)z^{*2}/(1 + \lambda) \quad (51b)$$

and z^* is given by eqn (39a) with $z' = 0$.

The springs 1 and 2 remain elastic for further motion provided

$$(1 - \lambda)z^*/(1 + \lambda) \leq z \leq z^*. \quad (52)$$

6. NUMERICAL STUDY OF DYNAMIC BEHAVIOR WITH $m_0 \neq 0$

The theoretical analyses in Sections 4 and 5 were developed for the model in Fig. 1(a) with $m_0 = 0$, while in this section a numerical procedure is used to explore the dynamic buckling response when $m_0 \neq 0$.

It is assumed, for convenience, that springs 1 and 2 have the same characteristics, which are indicated in Fig. 2 and may be expressed in the form

$$\dot{Q}_\alpha = \Psi_\alpha \dot{x}_\alpha / r^2, \quad \alpha = 1, 2, \quad (53)$$

where

$$x_\alpha = u_\alpha / L_2, \quad (54a)$$

$$x_1 = y - z(z + 2\bar{z}) - rz, \quad \text{and} \quad x_2 = y - z(z + 2\bar{z}) + rz \quad (54b, c)$$

from eqns (1) and (2). $\Psi_\alpha = 1$ when $\dot{Q}_\alpha < 0$, or when $Q_\alpha < Q_\alpha^{\max}$, where Q_α^{\max} is the largest dimensionless force subjected to spring α or the dimensionless yield load (Δ_j / rL_1) when no plastic flow has occurred. $\Psi_\alpha = \lambda$ when $Q_\alpha \geq Q_\alpha^{\max}$ and $\dot{Q}_\alpha > 0$ and provided $Q_\alpha^{\max} > \Delta_j / rL_1$.

Equations (3) may be written in the form

$$\epsilon y_m'' + r^2(Q_{1m} + Q_{2m})/2 = r^2 Q/2 \quad (55a)$$

and

$$z_m'' - (z_m + \bar{z})(Q_{1m} + Q_{2m}) - r(Q_{1m} - Q_{2m})/2 - az_m^2 = 0, \quad (55b)$$

where the subscript m implies evaluation of the variable at the dimensionless time τ_m and the external load is a step load of constant magnitude and infinite duration.

Equations (55) may be recast into a set of non-linear algebraic equations using finite-difference expressions[24] as shown in the accompanying Appendix. This set of equations was solved at each time step using a standard Newton-Raphson iterative procedure[25]. Further details of the numerical scheme are presented in the Appendix.

7. DISCUSSION

The phase plane portraits for the dynamic elastic-plastic and dynamic plastic-elastic cases are respectively drawn in Figs. 6 and 7 for a particular set of parameters with $m_0 = 0$. It is evident from both of these figures that the dynamic response of the model remains entirely elastic (i.e. model shakes down to an elastic state) after unloading from the state ($z' = 0$, $z = z^*$) provided $P \leq P_D$, where P_D is defined by eqns (34) and (39b). Thus, plastic behavior of the idealised column in Fig. 1(a) with $m_0 = 0$ occurs only during the first excursion of m_1 , with the subsequent vibrations remaining elastic when $P \leq P_D$.

A composite curve for the dimensionless dynamic buckling loads P_D/P_C associated with the dimensionless initial imperfections $a\bar{z}$ is plotted in Fig. 8 for a particular set of parameters and compared with the corresponding static buckling results taken from Fig. 4. Inequality (24) is an

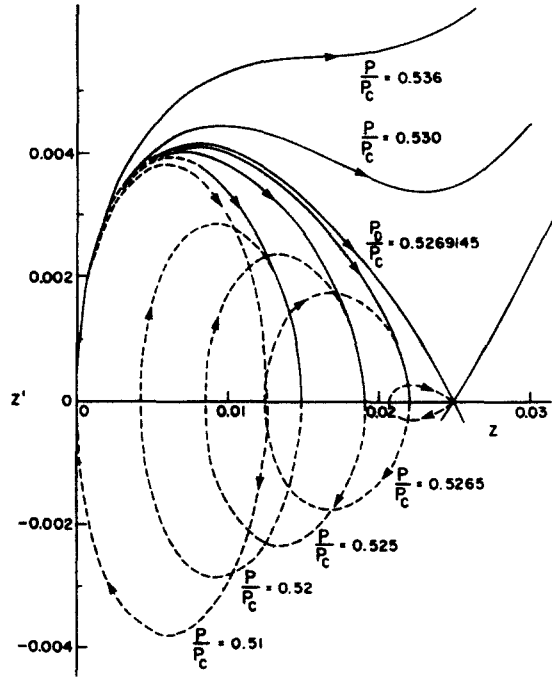


Fig. 6. Phase plane trajectories for the dynamic elastic-plastic case with $m_0=0$, $a=10$, $\lambda=0.75$, $a\bar{z}=0.05$, $r=1$ and $\Delta_1 L_2/L_1^2=0.268$. ----- elastic behavior, ——— eqn (32).

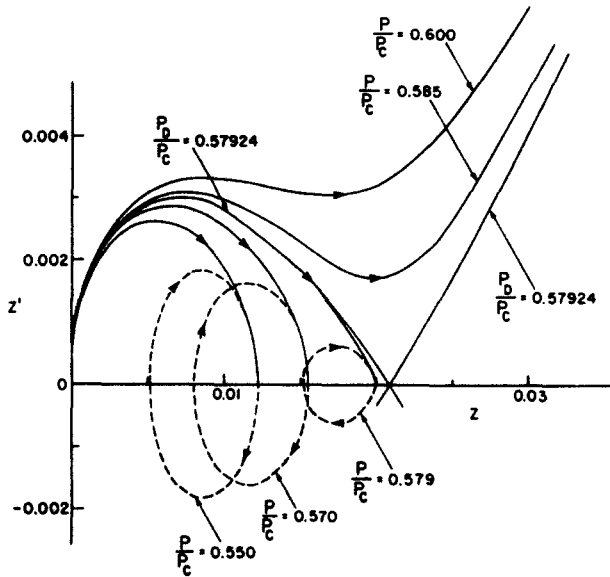


Fig. 7. Phase plane trajectories for the dynamic plastic-elastic case with $m_0=0$, $a=10$, $\lambda=0.75$ and $a\bar{z}=0.025$. ----- elastic behavior, ——— eqn (39).

equality at point c in Fig. 8 so that dynamic buckling of the model in Fig. 1 is controlled by wholly elastic effects for larger initial imperfections (i.e. curve cd), while inequality (36) is satisfied on the portion bc for which dynamic elastic-plastic buckling prevails. The point b is associated with the left hand side of equality (40). Thus, dynamic plastic-elastic buckling governs the behaviour of the model for small imperfections which lie on the curve ab . It is also evident that a model with large initial imperfections might buckle elastically when subjected to dynamic loads, while the same model with small initial imperfections would buckle plastically. Furthermore, initial imperfections are as important for dynamic plastic-elastic buckling as they are for dynamic elastic buckling (see also eqns 23 and 39b).

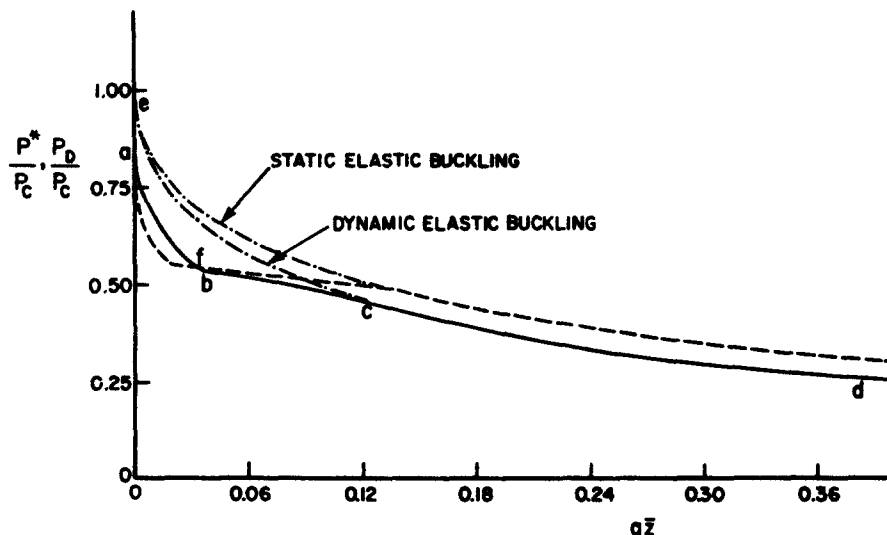


Fig. 8. Comparison of dynamic (P_D) and static (P^*) buckling loads when $m_0 = 0$, $a = 10$, $r = 1$, $\lambda = 0.75$ and $\Delta_y L_2/L_1^2 = 0.268$. —, :Static; - - -, dynamic: eqn (23) (ed, elastic), eqn (34) (bc, elastic-plastic) and eqn (39b) (ab, plastic-elastic).

The sequence of plastic loading and elastic unloading in springs 1 and 2 are different for the static and dynamic loading cases shown in Fig. 8. If the initial imperfection is sufficiently small in the static case, then both springs respond elastically until spring 2 yields plastically. Loading continues with spring 1 elastic and spring 2 plastic until spring 1 yields plastically. Further static loading continues with both springs responding plastically until spring 1 commences to unload elastically. Finally, spring 2 continues to load plastically and spring 1 unloads elastically from its earlier plastic state until the maximum load carrying capacity is reached.

The dynamic buckling load according to eqn (39b) for a perfect model equals the reduced modulus load ($2\Omega P_c$) because the inertia of the prebuckling response is neglected (i.e. $m_0 = 0$). Thus, the external step loading P can be accommodated by springs 1 and 2 prior to any lateral movement (ξ) of mass m_1 . In fact, the immediate response of both springs 1 and 2 is identical for a given value of P , regardless of whether the model is initially perfect ($a\bar{z} = 0$) or has initial stress-free imperfections ($a\bar{z} \neq 0$). The dynamic buckling loads in Fig. 8 are therefore larger than the corresponding static ones for small imperfections which is due largely to the different elastic-plastic deformation histories in the springs during the static and dynamic responses. It should be noted that Hartzman[9] found that the dynamic buckling pressure of a geometrically perfect elastic-plastic spherical dome was larger than the corresponding static buckling pressure. However, the dynamic buckling loads for the model in Fig. 1(a) are smaller than the associated static ones when the initial imperfections are larger than those corresponding to point f in Fig. 8.

It is interesting to observe from the particular curves in Fig. 8 for models with initial imperfections lying within the range $0.1230 \leq a\bar{z} \leq 0.1372$ that static loads cause plastic buckling while dynamic loads are responsible for elastic buckling.

A typical growth of the dimensionless displacement z^* with the magnitude of the step load P is shown in Fig. 9 for the elastic case according to eqn (22). The amplitude of z^* is unbounded when $P = P_D$ because the static post-buckling characteristics of the idealised model shown in Figs. 3 and 9 are always unstable. The dynamic buckling load when plasticity occurs in the model is not given by the intersection of the static and dynamic curves as shown for the elastic case in Fig. 9, largely because the history of loading and unloading of springs 1 and 2 are different for the two cases.

It is evident from Fig. 10 that the material strain hardening parameter (λ) exercises an important effect on the dynamic buckling characteristics and the model is more imperfection-sensitive for smaller values of λ .

The theoretical results discussed above and presented in Figs. 5–10 were obtained using the analytical method outlined in Sections 4 and 5 which was simplified by taking $m_0 = 0$. In order

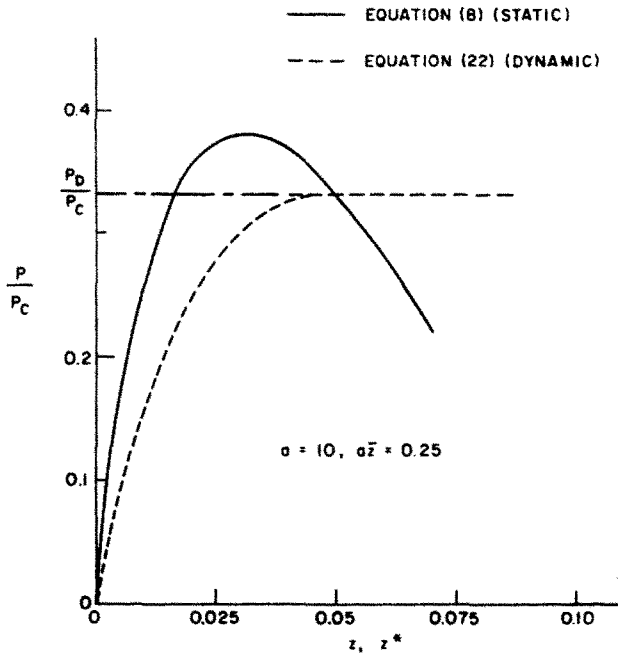


Fig. 9. Growth of maximum amplitude of z with P/P_c according to eqns (8) and (22) for the static elastic and dynamic elastic cases with $a = 10, a\bar{z} = 0.25$ and $m_0 = 0$.

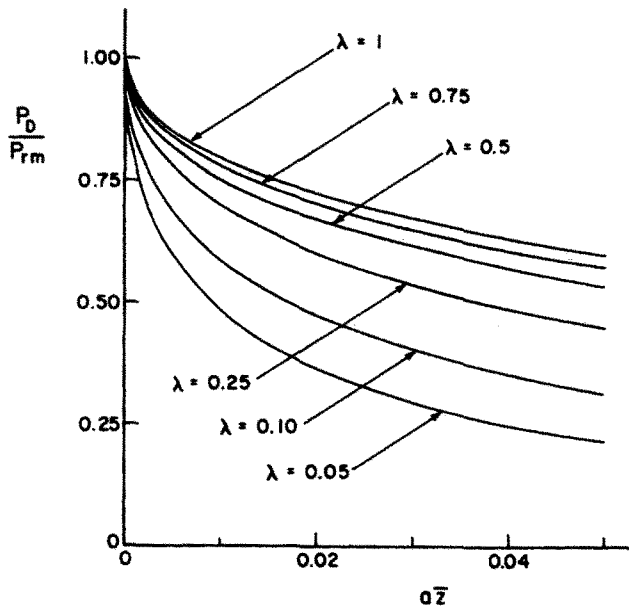


Fig. 10. Influence of material strain hardening ratio (λ) on dynamic plastic-elastic buckling when $m_0 = 0$ according to eqn (39b).

to explore the influence of m_0 , or ω_1/ω_0 , the method in Section 6 was used to obtain the numerical results presented in Figs. 11–19.

The variation of z with dimensionless time τ is shown in Fig. 11 when $\omega_1/\omega_0 = 0.316$. It is evident that a high frequency oscillation is superposed on a dominant mode which represents a lateral vibration of the idealised column about a deformed state. The period of the dominant mode grows as the vertical load P is increased until the dynamic buckling load P_D/P_c is reached when a form of “direct” buckling[26] occurs and the amplitude of z (i.e. z^*) becomes unbounded as indicated in Fig. 13 for several values of the dimensionless imperfection (\bar{z}). The temporal variation of the dimensionless vertical displacement y shown in Fig. 12 is ap-

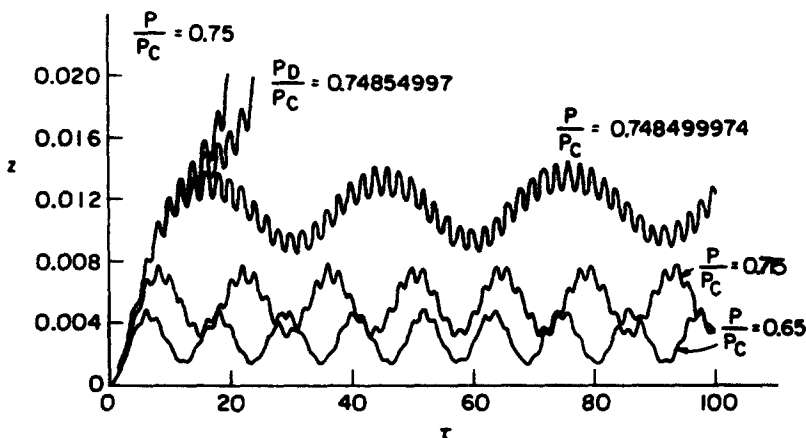


Fig. 11. Variation of dimensionless displacement (z) with dimensionless time τ for $\omega_1/\omega_0 = 0.316$, $\lambda = 0.75$, $4\alpha\beta/\lambda = 0.05$, $r = 1$, $\Delta_p L_2/L_1^2 = 0.268$ and $\Delta\tau = 0.025$.

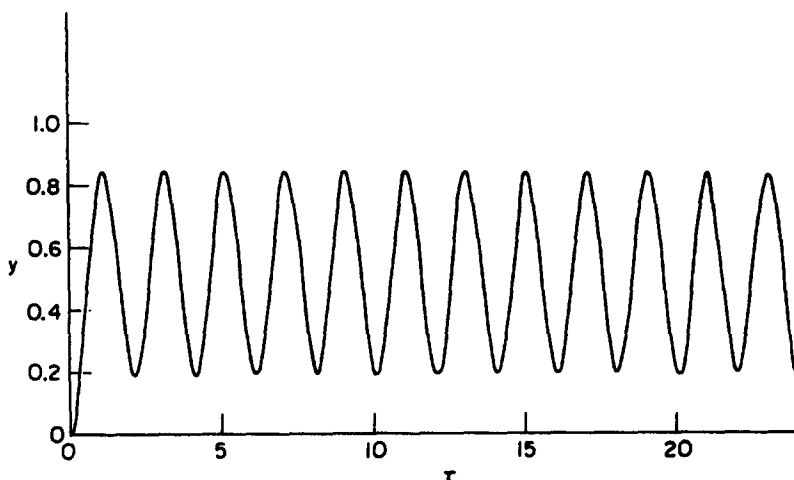


Fig. 12. Variation of dimensionless displacement (y) with dimensionless time τ for $\omega_1/\omega_0 = 0.316$, $\lambda = 0.75$, $4\alpha\beta/\lambda = 0.05$, $r = 1$, $\Delta_p L_2/L_1^2 = 0.268$, $P_D/P_C = 0.748549974274$ and $\Delta\tau = 0.025$.

proximately two orders of magnitude larger than z and does not reflect any growth when $P = P_D$ so that u_1 , u_2 , and u given by eqns (1a), (1b) and (2) would remain largely unaffected. The dimensionless dynamic buckling load when $\omega_1/\omega_0 = 0.316$ in Fig. 14 is sensitive to the magnitude of the dimensionless imperfection for both the elastic and elastic-plastic cases. In fact, because of the factor $1/\lambda$ in the abscissa, the idealised column in Fig. 1 is more imperfection sensitive for dynamic buckling loads which cause an elastic-plastic response than for those producing a wholly elastic behaviour.

The character of the response in Fig. 15 for $\omega_1/\omega_0 = 0.75$ is different to that when $\omega_1/\omega_0 = 0.316$. In this case, high frequency vibrations are superposed on a dominant mode having a very large period. The total duration of the numerical calculations is therefore important and the buckling load was obtained in the present calculations as the smallest load which caused z to exceed a specified value of z^* within the interval $0 < \tau < 100$. This type of behavior is similar to the "indirect" buckling phenomenon examined by Lock [26], who examined a dynamic elastic buckling problem and the results in Fig. 17 indicate the rapid growth of z^* as P is increased towards the dynamic buckling loads found in the current study. Again, the amplitude of the y displacements in Fig. 16 are approximately two orders of magnitude larger than z and are insensitive to the dramatic changes of z near the dynamic buckling load. It is apparent from Fig. 18 that the results for the idealised model are less imperfection-sensitive for "indirect" buckling when $\omega_1/\omega_0 = 0.75$ than the "direct buckling results for $\omega_1/\omega_0 = 0.316$ in Fig. 14.

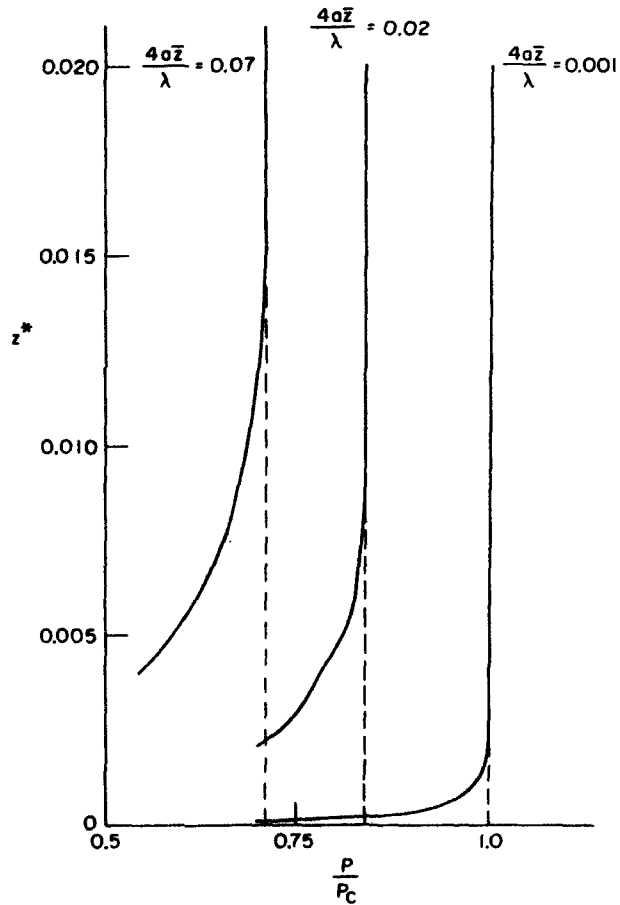


Fig. 13. Growth of maximum value of $z(z^*)$ with dimensionless load (P/P_c) for $\omega_1/\omega_0 = 0.316$, $\lambda = 0.75$, $r = 1$, $\Delta_1 L_2/L_1^2 = 0.268$ and $\Delta\tau = 0.025$.

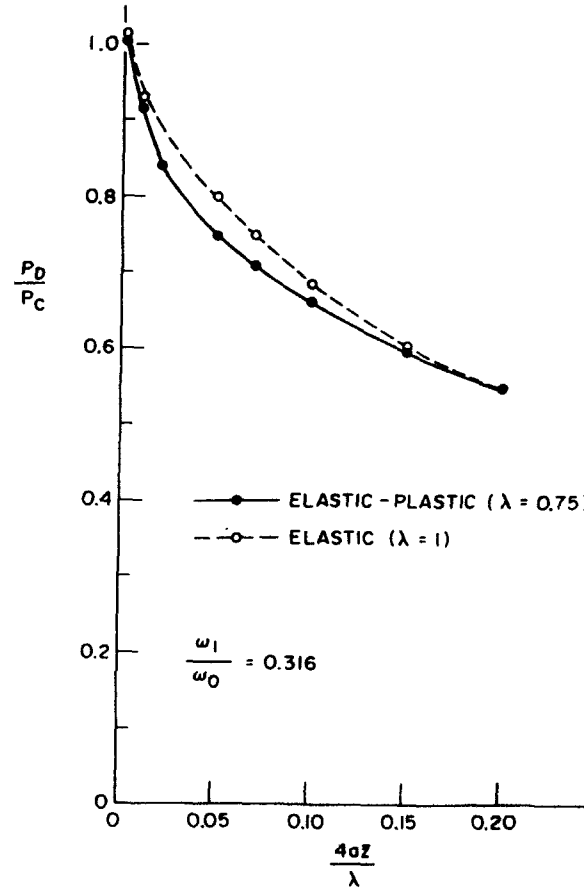


Fig. 14. Variation of dimensionless dynamic buckling load (P_D/P_c) with dimensionless initial geometric imperfection (Z) for elastic ($\lambda = 1$) and elastic-plastic ($\lambda = 0.75$) cases with $\omega_1/\omega_0 = 0.316$, $r = 1$, $\Delta_1 L_2/L_1^2 = 0.268$ and $\Delta\tau = 0.025$.

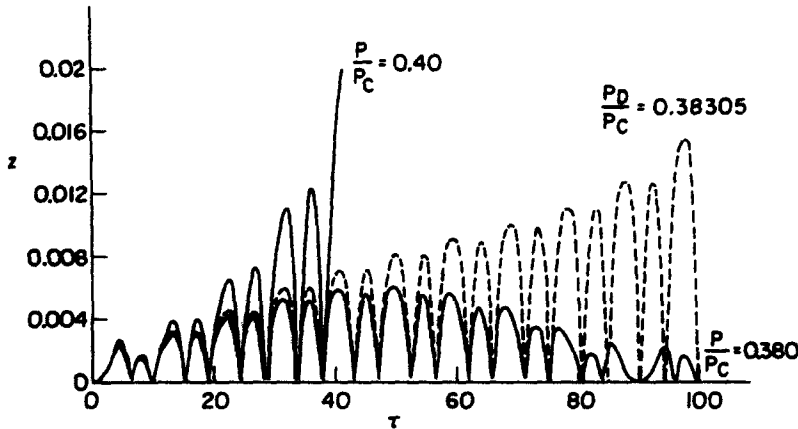


Fig. 15. Variation of dimensionless displacement (z) with dimensionless time τ for $\omega_1/\omega_0 = 0.75$, $\lambda = 0.75$, $4az/\lambda = 0.05$, $r = 1$, $\Delta_\gamma L_2/L_1^2 = 0.268$ and $\Delta\tau = 0.05$.

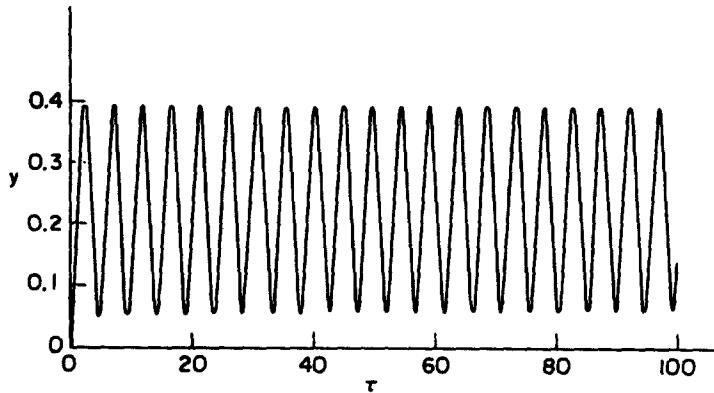


Fig. 16. Variation of dimensionless displacement (y) with dimensionless time (τ) for $\omega_1/\omega_0 = 0.75$, $\lambda = 0.75$, $4az/\lambda = 0.05$, $r = 1$, $\Delta_\gamma L_2/L_1^2 = 0.268$, $P_D/P_c = 0.383050005$ and $\Delta\tau = 0.05$.

The numerical values are summarised in Fig. 19 and the "direct" form of buckling (e.g. Fig. 11) is typical of the behaviour when $0 < \omega_1/\omega_0 < 0.5$, while the "indirect" type of dynamic buckling illustrated in Fig. 15 is typical of the response when $0.5 < \omega_1/\omega_0 < 1$. The sensitivity of the dynamic buckling load to the magnitude of the time step $\Delta\tau$ used in the numerical study is also indicated in Fig. 19 when $\omega_1/\omega_0 = 0.316$. However, the numerical results appear to be less sensitive for the "indirect" buckling case because, when $\omega_1/\omega_0 = 0.75$ and the values of the remaining parameters are given in the title of Fig. 19, the dimensionless buckling load (P_D/P_c) is 0.38165, 0.38155, and 0.38305 for dimensionless time steps ($\Delta\tau$) of 0.02, 0.03 and 0.05, respectively.

The general form of the numerical results in Fig. 19 is similar to that found by Danielson [20] for the wholly elastic case. In fact, Danielson's approximate theoretical result for $0 \leq \omega_1/\omega_0 \leq 0.5$ is the same as eqn (23) here which predicts $P_D/P_c = 0.8$ for the parameters used in Fig. 19. Danielson's approximate theoretical predictions for the range $0.5 \leq \omega_1/\omega_0 < 1.0$ is given by eqn (16b) in Ref. [20] which lies slightly below the numerical values in Fig. 19.

The numerical calculations demonstrate the extremely complicated dynamic buckling behaviour of the simple idealised model illustrated in Fig. 1 when subjected to a step loading which is the most severe form of loading according to Kao and Perrone [13]. As already remarked, the dynamic buckling load is sensitive to the duration of the numerical calculations (i.e. maximum value of τ) which is particularly evident in Fig. 15 for the "indirect" buckling case and to a lesser extent for the "direct" buckling behaviour in Fig. 11. In addition, the maximum acceptable values of $z(z^*)$ must be specified in order to determine a dynamic buckling load. The numerical results in Figs. 11–19 were obtained with either $z^* = 0.015$ or $z^* = 0.02$ and Figs. 13 and 17 indicate that the dynamic buckling loads are insensitive to the values of z^* having these magnitudes. However, the magnitude of the dynamic buckling load would be sensitive for smaller values of z^* , while the dimensionless time τ when the dynamic

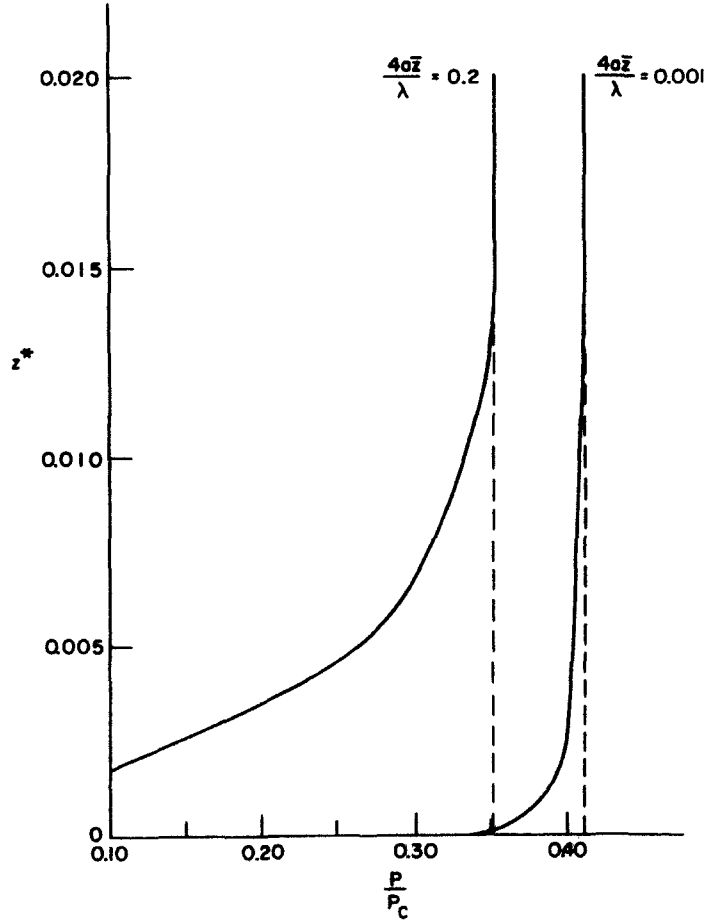


Fig. 17. Growth of maximum value of $z(z^*)$ with dimensionless load (P/P_c) for $\omega_1/\omega_0 = 0.75$, $\lambda = 0.75$, $r = 1$, $\Delta_y L_2/L_1^2 = 0.268$ and $\Delta\tau = 0.05$.

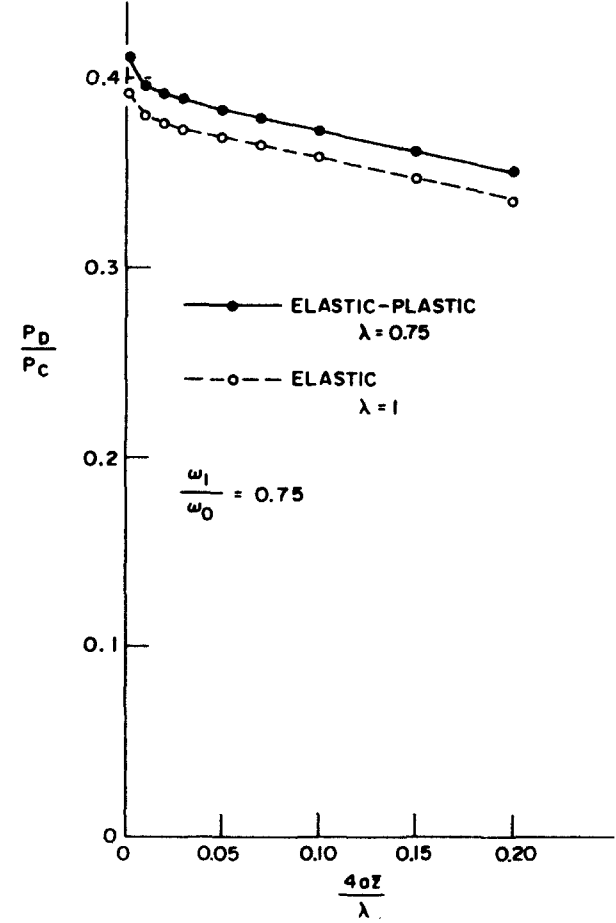


Fig. 18. Variation of dimensionless dynamic buckling load (P_D/P_C) with dimensionless initial geometric imperfection (z) for $\omega_1/\omega_0 = 0.75$, $r = 1$, $\Delta_y L_2/L_1^2 = 0.268$ and $\Delta\tau = 0.05$.

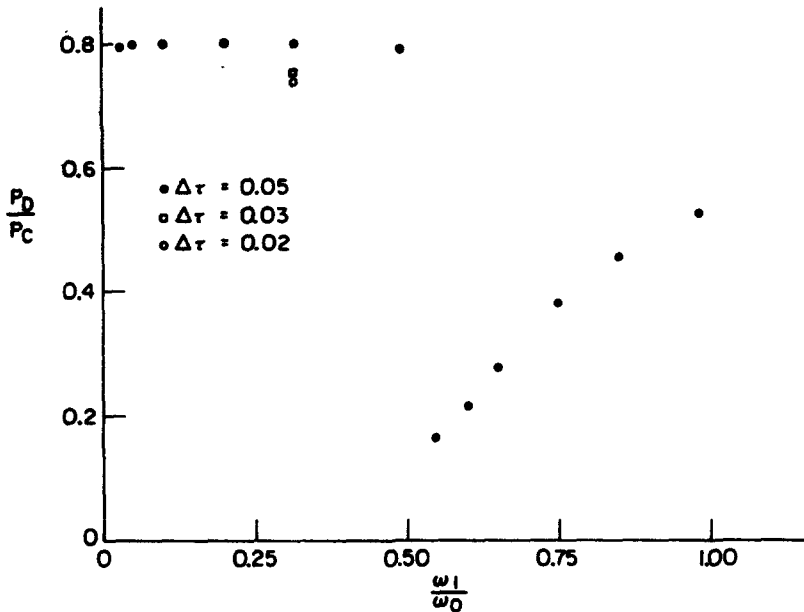


Fig. 19. Variation of dimensionless dynamic buckling load (P_D/P_C) with frequency ratio ω_1/ω_0 for $4a\beta/\lambda = 0.05$, $\lambda = 0.75$, $\Delta_p L_2/L_1^2 = 0.268$ and $r = 1$.

buckling load is reached would be sensitive to z^* regardless of its value. Thus, it is important to specify the values of z^* and τ_{\max} associated with the numerical calculations of a dynamic buckling load.

A comparison between Figs. 8 and 14 reveals that the dynamic elastic-plastic results with $m_0 \neq 0$ lie above the corresponding static elastic-plastic values, a circumstance which was also found when $m_0 = 0$ for initial imperfections smaller than those corresponding to point *f* in Fig. 8. The dynamic elastic buckling curves in Figs. 8 and 14 both lie below the corresponding static elastic values. It is evident from Figs. 8 and 18 that due to the different nature of the buckling response both dynamic results in Fig. 18 lie below the corresponding static values. The dynamic elastic-plastic buckling curves in Fig. 18 lie above the associated dynamic elastic results when $\omega_1/\omega_0 = 0.75$ a phenomenon which was not predicted by the simple theoretical analysis with $m_0 = 0$ ($\omega_1/\omega_0 = 0$) for "direct" buckling in Section 4.

The influence of damping was neglected in the present study. Lock [26] examined the effect of viscous damping in his theoretical investigations on the elastic instability of a shallow sinusoidal arch. Damping was found to reduce the "indirect" snapping pressure and to be responsible for an increase in the "direct" snapping pressure. In other words, the dynamic buckling pressures were closer to the corresponding critical static pressures than were those without damping and the effect was particularly marked for the "indirect" snapping case. In the present study, the dynamic buckling loads are less than the corresponding static loads except for the "direct" dynamic elastic-plastic instability results in Fig. 14 for $\omega_1/\omega_0 = 0.316$ and the dynamic plastic-elastic results with imperfections smaller than those at *f* in Fig. 8.

It is important to emphasise that the theoretical predictions and discussion herein refer only to the idealised model shown in Fig. 1(a) with a restricted range of parameters. However, it might be expected that some features of the response would be reflected in the dynamic behaviour of actual structures as already remarked with regard to Hartzman's [9] numerical investigation on a spherical dome.

8. CONCLUSIONS

The imperfection-sensitive idealised model illustrated in Fig. 1, which has elastic-plastic springs to simulate material plasticity, was subjected to a step loading and the response examined using theoretical and numerical methods. An exact theoretical solution was developed in Sections 4 and 5 for the particular case when $m_0 = 0$ (i.e. $\omega_1/\omega_0 = 0$), while a numerical scheme was presented in Section 6 for the more general case when $\omega_1/\omega_0 \neq 0$.

It was found that the stable response of the model with $m_0 = 0$ shakes down to an elastic

state after any plastic behaviour during the first excursion of m_1 . Dynamic plastic-elastic buckling governs the response for small initial imperfections, while instability occurs elastically for large imperfections. It transpires that the dynamic buckling load of a model with small imperfections is larger than the corresponding static buckling load because of the different elastic-plastic deformation histories in the springs during the static and dynamic responses.

The numerical study for a model with $m_0 \neq 0$ (i.e. $\omega_1/\omega_0 \neq 0$) reveals two different types of dynamic buckling which are similar to those observed by Lock[26] for a dynamic elastic buckling problem. A "direct" form of dynamic instability occurs when $0 \leq \omega_1/\omega_0 \leq 0.5$ while an "indirect" type is associated with $0.5 \leq \omega_1/\omega_0 \leq 1.0$.

The various results presented herein indicate that dynamic plastic buckling is imperfection-sensitive particularly for "direct" buckling within the range $0 \leq \omega_1/\omega_0 \leq 0.5$.

Acknowledgements—The authors wish to record their gratitude to Dr. N. Perrone and Dr. N. Basdekas of the Structural Mechanics Program of O.N.R. who largely supported this investigation through contract number N00014-76-C-0195, Task NR 064-510. The authors are also indebted to Mr. E. A. Papageorgiou who assisted with the numerical calculations.

REFERENCES

1. J. N. Goodier, Dynamic plastic buckling. *Proc. Int. Conf. on Dynamic Stability of Structures* (Edited by G. Herrmann), pp. 189-211. Pergamon Press, Oxford (1967).
2. J. N. Goodier, Dynamic buckling of rectangular plates in sustained plastic compressive flow. *Engineering Plasticity* (Edited by J. Heyman and F. A. Leckie), pp. 183-200. Cambridge University Press (1968).
3. H. Ramsey and H. Vaughan, Dynamic elastic-plastic buckling of rectangular plates in sustained flow. *Quart. Appl. Math.* 28(4), 473-487 (1971).
4. A. L. Florence and J. N. Goodier, Dynamic plastic buckling of cylindrical shells in sustained axial compressive flow. *J. Appl. Mechs.* 35, 80-86 (1968).
5. H. Vaughan and A. L. Florence, Plastic flow buckling of cylindrical shells due to impulsive loading. *J. Appl. Mechs.* 37, 171-179 (1970).
6. N. Jones and D. M. Okawa, Dynamic plastic buckling of rings and cylindrical shells. *Nucl. Engng and Design* 37, 125-147 (1976).
7. N. Jones and C. S. Ahn, Dynamic buckling of complete rigid-plastic spherical shells. *J. Appl. Mechs.* 41, 609-614 (1974).
8. N. Jones and C. S. Ahn, Dynamic elastic and plastic buckling of complete spherical shells. *Int. J. Solids Structures* 10, 1357-1374 (1974).
9. M. Hartzman, Comparison of calculated static and dynamic collapse pressures for clamped spherical domes. *AIAA J.* 12, 568-570 (1974).
10. K.-J. Bathe, E. Ramm and E. L. Wilson, Finite element formulations for large deformation dynamic analysis. *Int. J. Numer. Meth. in Engng.* 9, 353-386 (1975).
11. L. Morino, J. W. Leech and E. A. Witmer, An improved numerical calculation technique for large elastic-plastic transient deformations of thin shells—I,II. *J. Appl. Mechs.* 38, 423-436 (1971).
12. J. T. Oden, and K.-J. Bathe, A commentary on computational mechanics. *Appl. Mechs. Revs.* 31, 1053-1058 (1978).
13. R. Kao and N. Perrone, Dynamic buckling of axisymmetric spherical caps with initial imperfections. *Comput. and Structures* 9, 463-473 (1978).
14. F. R. Shanley, Inelastic column theory. *J. Aero. Sci.* 14, 261-268 (1947).
15. M. J. Sewell, The static perturbation technique in buckling problems. *J. Mech. Phys. Solids* 13, 247-265 (1965).
16. J. W. Hutchinson, On the postbuckling behavior of imperfection-sensitive structures in the plastic range. *J. Appl. Mechs.* 39, 155-162 (1972).
17. B. Budiansky and J. W. Hutchinson, Dynamic buckling of imperfection-sensitive structures. *Proc. 11th Int. Cong. Appl. Mechs.* (Edited by H. Görtler), pp. 636-651. Springer-Verlag, Berlin (1964).
18. J. W. Hutchinson and B. Budiansky, Dynamic buckling estimates. *AIAA J.* 4, 525-530 (1966).
19. B. Budiansky, Dynamic buckling of elastic structures: criteria and estimates. *Proc. Int. Conf. on Dynamic Stability of Structures* (Edited by G. Herrmann), pp. 83-106. Pergamon Press, Oxford (1967).
20. D. A. Danielson, Dynamic buckling loads of imperfection-sensitive structures from perturbation procedures. *AIAA J.* 7, 1506-1510 (1969).
21. N. C. Huang and W. T. Tsai, Dynamic snap-through of an elastic-plastic simple shallow truss. *Int. J. Solids Structures* 5, 737-753 (1969).
22. D. Graham and D. McRuer, *Analysis of nonlinear control systems*. Dover (1971).
23. H. T. Davis, *Introduction to Nonlinear Differential and Integral Equations*. Dover (1962).
24. J. C. Houbolt, A recurrence matrix solution for the dynamic response of aircraft in gusts. *NACA Rep.* 1010 (1951).
25. B. Carnahan, H. A. Luther and J. O. Wilkes, *Applied Numerical Methods*. Wiley, New York (1969).
26. M. H. Lock, Snapping of a shallow sinusoidal arch under a step pressure load. *AIAA J.* 4, 1249-1256 (1966).

APPENDIX

This appendix contains the details of the numerical scheme used to solve eqns (55).

Now, for sufficiently small time increments, the dimensionless forces in springs 1 and 2 at the dimensionless time τ_m are related to the forces in the springs at τ_{m-1} in the following manner:

$$Q_{am} = Q_{a(m-1)} + \Psi_a \{x_{am} - x_{a(m-1)}\}/r^2 \quad (A1)$$

which when using eqns (54) give

$$Q_{1m} + Q_{2m} = A + (C y_m - C z_m^2 - E z_m - G) / r^2 \tag{A2a}$$

$$Q_{1m} - Q_{2m} = B + (D y_m - D z_m^2 - F z_m - H) / r^2 \tag{A2b}$$

where

$$\begin{aligned} A &= Q_{1(m-1)} + Q_{2(m-1)}, & B &= Q_{1(m-1)} - Q_{2(m-1)}, \\ C &= \Psi_1 + \Psi_2, & D &= \Psi_1 - \Psi_2, & E &= \Psi_1(2\bar{x} + r) + \Psi_2(2\bar{x} - r), \\ F &= \Psi_1(2\bar{x} + r) - \Psi_2(2\bar{x} - r), & G &= \Psi_1 x_{1(m-1)} + \Psi_2 x_{2(m-1)}, \\ H &= \Psi_1 x_{1(m-1)} - \Psi_2 x_{2(m-1)}. \end{aligned} \tag{A3a-h}$$

The dimensionless accelerations in eqns (55) are approximated using Houbolt's third order backwards finite-difference scheme[24]

$$y_m'' = (\alpha_m y_m + \beta_m y_{m-1} + \gamma_m y_{m-2} + \delta_m y_{m-3}) / (\Delta\tau)^2 + Y_m \tag{A4}$$

and a similar expression for z_m'' with Z_m instead of Y_m , where $\Delta\tau$ is the dimensionless time step, and the coefficients $\alpha_m = 2$, $\beta_m = -5$, $\gamma_m = 4$, $\delta_m = -1$ and $Y_m = Z_m = 0$ provided $m \geq 3$ when $m = 0$ refers to the initial conditions at $\tau = 0$. Now the fictitious deflections y_{-1} and y_{-2} may be expressed in terms of y_0 , y'_0 , y''_0 and y_1 by using standard finite-difference expressions for y'_0 and y''_0 (e.g. eqns (B3) and (B7) in Ref.[24]). It turns out with the initial conditions $y_0 = y'_0 = 0$ and $y''_0 = r^2 Q / 2\epsilon$ that $\alpha_0 = \beta_0 = \gamma_0 = \delta_0 = 0$, $Y_0 = y''_0$, $\alpha_1 = -\beta_1 = 6$, $\gamma_1 = \delta_1 = 0$, $Y_1 = -r^2 Q / \epsilon$, $\alpha_2 = \gamma_2 = 2$, $\beta_2 = -4$, $\delta_2 = 0$ and $Y_2 = -Y_1 / 2$. Similar results are obtained for z_m'' except $z''_0 = 0$ giving $Z_0 = Z_1 = Z_2 = 0$.

Thus, substituting eqns (A2) and (A4) into eqns (55) gives a set of non-linear algebraic equations which were solved at each time step using a standard Newton-Raphson iterative procedure[25]. For this purpose the algebraic equations were recast in the form

$$\begin{bmatrix} a_{11} & a_{12} \\ a_{21} & a_{22} \end{bmatrix}_{j,m} \begin{Bmatrix} \delta y \\ \delta z \end{Bmatrix}_{j,m} = \begin{Bmatrix} P_1 \\ P_2 \end{Bmatrix}_{j,m} \tag{A5}$$

where $y_m^{j+1} = y_m^j + \delta y_m^j$ and $z_m^{j+1} = z_m^j + \delta z_m^j$ when j is the j iteration cycle at dimensionless time $\tau_m = m \Delta\tau$ and

$$\begin{aligned} a_{11} &= \epsilon \alpha_m / (\Delta\tau)^2 + C / 2, & a_{12} &= -C z_m^j - E / 2, \\ a_{21} &= -C(\bar{x} + z_m^j) / r^2 - D / 2r, \\ a_{22} &= \alpha_m / (\Delta\tau)^2 - A - (C y_m^j - C z_m^j - E z_m^j - G) / r^2 \\ &\quad + (2C z_m^j + E)(z_m^j + \bar{x}) / r^2 + (2D z_m^j + F) / 2r - 2a z_m^j, \\ P_1 &= -\epsilon(\alpha_m y_m^j + \beta_m y_{m-1}^j + \gamma_m y_{m-2}^j + \delta_m y_{m-3}^j) / (\Delta\tau)^2 \\ &\quad - \epsilon Y_m - r^2 A / 2 - (C y_m^j - C z_m^j - E z_m^j - G) / 2 + r^2 Q / 2, \\ P_2 &= -(\alpha_m z_m^j + \beta_m z_{m-1}^j + \gamma_m z_{m-2}^j + \delta_m z_{m-3}^j) / (\Delta\tau)^2 - Z_m + a z_m^j \\ &\quad + (z_m^j + \bar{x}) \{ A + (C y_m^j - C z_m^j - E z_m^j - G) / r^2 \} \\ &\quad + r B / 2 + (D y_m^j - D z_m^j - F z_m^j - H) / 2r. \end{aligned} \tag{A6a-f}$$

The iterations were terminated at τ_m when

$$\{[(\delta y_m^j)^2 + (\delta z_m^j)^2] / \{(y_m^j)^2 + (z_m^j)^2\}\}^{1/2} \leq 10^{-15}. \tag{A7}$$